

---

# FC-GAGA: Fully Connected Gated Graph Architecture for Spatio-Temporal Traffic Forecasting

---

**Boris N. Oreshkin**  
boris.oreshkin@gmail.com

**Arezou Amini**  
McGill University  
arezou.amini@mail.mcgill.ca

**Lucy Coyle**  
McGill University  
lucy.coyle@mail.mcgill.ca

**Mark J. Coates**  
McGill University  
mark.coates@mcgill.ca

## Abstract

Forecasting of multivariate time-series is an important problem that has applications in many domains, including traffic management, cellular network configuration, and quantitative finance. In recent years, researchers have demonstrated the value of applying deep learning architectures for these problems. A special case of the problem arises when there is a graph available that captures the relationships between the time-series. In this paper we propose a novel learning architecture that achieves performance competitive with or better than the best existing algorithms, without requiring knowledge of the graph. The key elements of our proposed architecture are (i) jointly performing backcasting and forecasting with a deep fully-connected architecture; (ii) stacking multiple prediction modules that target successive residuals; and (iii) learning a separate causal relationship graph for each layer of the stack. We can view each layer as predicting a component of the time-series; the differing nature of the causal graphs at different layers can be interpreted as indicating that the multivariate predictive relationships differ for different components. Experimental results for two public traffic network datasets illustrate the value of our approach, and ablation studies confirm the importance of each element of the architecture.

## 1 Introduction

Many multivariate time-series (TS) forecasting problems naturally admit a graphical model formulation. This is especially true when the entities whose past is observed and whose future has to be predicted affect each other through simple causal relationships. For example, introducing pepsi products in a store will very likely decrease future sales of coca-cola in that store; car traffic congestion at one point on a highway is likely to slow down the traffic at preceding segments of the highway. Without graphical modeling, the model is blind to these nuances, making entity interactions a collection of confounding factors, extremely hard for the model to explain and predict. Equipped with a learnable model for entity properties (e.g. entity embeddings), a model for entity interactions (e.g. graph edge weights), and a mechanism to connect those to a TS model (e.g. a gating mechanism), we can attempt to learn the otherwise unknown entity interactions to improve forecasting accuracy.

Problems amenable to graphical TS modeling include forecasting demand for related products [33], electricity demand [28], road traffic [32] or passenger demand [2]. Recent studies have shown that models that explicitly account for the underlying relationships across multiple TS outperform models that forecast each TS in isolation. Although the inclusion of graph modeling has proven to improve accuracy, current models have several serious limitations. First, the complexity and therefore runtime

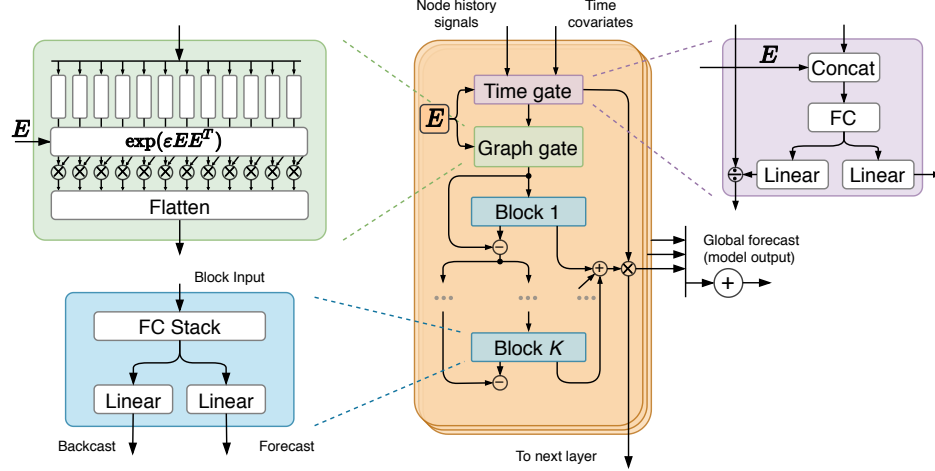


Figure 1: FC-GAGA block diagram

of these models is significantly higher. Second, some models rely on the definition of relationships between variables provided by a domain expert (e.g. an adjacency matrix is heuristically defined based on the geographical relationships between observed variables). Finally, existing models tend to rely on Markovian assumptions to make modelling the interactions across variables tractable.

To address these limitations we propose a novel architecture, called FC-GAGA, that is based on a combination of a fully-connected TS model and a graph gate mechanism. To produce the forecast for a single TS (node in the graphical model), it weighs the historical observations of all other nodes by learnable graph weights, gates them via a ReLU and then stacks gated observations of all nodes to process them via fully connected residual blocks (see Fig. 1). The advantages of this architecture are threefold. First, the architecture does not rely on the knowledge of the underlying graph and instead learns all the required node relations. It focuses on predictive relationships, as opposed to correlations, and they can be nonlinear in nature. Second, the basic layer of the architecture is stackable and we allow every layer to learn its own graph structure. This makes the model of information diffusion across TS very general and non-Markovian. Yet, we empirically show that it can be learned effectively, resulting in excellent generalization performance. Finally, FC-GAGA has a streamlined architecture rich in human-interpretable components that is very memory and computation efficient, which we demonstrate via profiling.

### 1.1 Problem statement

Let a graph  $G = (V, E)$  be defined as an ordered collection of vertices,  $V = 1, \dots, N$ , and edges,  $E \subset V \times V$ . We are interested in the multivariate TS forecasting problem defined on this graph. Each vertex  $v$  in the graph is assumed to generate a sequence of observations,  $\mathbf{y}_v = [y_{v,1}, \dots, y_{v,T}] \in \mathbb{R}^T$ , governed by an unknown stochastic random process. The graph connectivity encoded in  $E$  is assumed to capture unknown causal relations between the vertices. For example, the graph edges  $E$  may encode the node connectivity in a wireless network and  $\mathbf{y}_v$  may be the observations of the number of transferred packets, or  $E$  may reflect the connectivity of roads in a road network and  $\mathbf{y}_v$  may be the sequence of observations of traffic velocity. The task is to predict the vector of future values  $\mathbf{y}_v \in \mathbb{R}^H = [y_{v,T+1}, y_{v,T+2}, \dots, y_{v,T+H}]$  for every vertex  $v$  based on the observations generated by all the vertices in the graph up to time  $T$ . For simplicity, we will later consider a *lookback window* of length  $w \leq T$  ending with the last observed value  $y_{v,T}$  to serve as model input, and denoted  $\mathbf{X}_v \in \mathbb{R}^w = [y_{v,T-w+1}, \dots, y_{v,T}]$ . We denote  $\hat{\mathbf{y}}_v$  the point forecast of  $\mathbf{y}_v$  at vertex  $v$ .

**Metrics:** The accuracy of our model is measured with three widely used metrics: Mean Absolute Error (MAE), Mean Absolute Percentage Error (MAPE), and Root Mean Squared Error (RMSE):

$$\text{MAE} = \frac{1}{N} \sum_{v=1}^N |y_{v,T+H} - \hat{y}_{v,T+H}|, \text{MAPE} = \frac{1}{N} \sum_{v=1}^N \frac{|y_{v,T+H} - \hat{y}_{v,T+H}|}{|y_{v,T+H}|}, \text{RMSE} = \sqrt{\frac{1}{N} \sum_{v=1}^N (y_{v,T+H} - \hat{y}_{v,T+H})^2}.$$

## 1.2 Summary of Contributions

We propose and empirically validate a novel neural network architecture for modelling multiple TS related via an unknown graph. The architecture is based on a novel principle of combining a fully connected TS model with learnable time and graph based gating mechanisms. The proposed architecture offers two main advantages over existing approaches. First, the proposed graph gate mechanism is not based on a node proximity model and is therefore more general than the currently prevalent Markovian models. We empirically show that the proposed model learns the required graph parameters effectively from the data and demonstrate state of the art performance of the proposed model. Second, we show that the proposed model offers computational advantage and reduces the training time by at least a factor of three relative to models with similar accuracy.

## 2 FC-GAGA

The high-level block diagram of the proposed architecture is presented in Fig. 1. We model node  $i$  in the underlying graph by representing it as an embedding vector of dimensionality  $d$ ,  $\mathbf{e}_i = [e_{i,1}, \dots, e_{i,d}]$ . The collection of all such vectors comprises node embedding matrix  $\mathbf{E} \in \mathbb{R}^{N \times d}$ . In the following, we describe the operation of a single layer, dropping the layer index for clarity.

**Graph edge weights:** The strengths of node links are encoded in a weight matrix  $\mathbf{W} \in \mathbb{R}^{N \times N}$  derived from node embeddings:

$$\mathbf{W} = \exp(\varepsilon \mathbf{E} \mathbf{E}^T). \quad (1)$$

Here  $\varepsilon$  is a parameter that is set to allow for the decoupling of the scaling of  $\mathbf{E}$ , which is used in other parts of the architecture, from the scaling that is required to achieve the necessary dynamic range in  $\mathbf{W}$ . We expect that the magnitudes of edge weights  $\mathbf{W}_{i,j}$  will reflect the strength of mutual influence between the pair of nodes  $(i, j)$  at a given FC-GAGA layer.

**Time gate block:** The time gate block models the time covariate features (*e.g.* time-of-day, day-of-week, etc.) that may be available together with the node observations. In general, data with strong seasonal patterns (hour, day, week, etc.) require model components that are able to explicitly capture these effects. We propose to model time related features using a multiplicative gate model that divides/multiplies the input/output of the FC-GAGA layer by time effects derived from the time feature via a fully connected network as depicted in Fig. 1. Additionally, the input time feature vector is concatenated with the node embedding to account for the fact that each node may have a different seasonality pattern. This is equivalent to removing a node-specific multiplicative seasonality from the input of the block and applying it again at the output of the block. Often, time-related seasonality effects are best modelled using a multiplicative model, however, the proposed approach is trivially extendable to accommodate for the additive case. We allow the input and output time effects to be decoupled via separate linear projection layers, because in general time at the input and at the output is different.

**Graph gate block:** The input to the FC-GAGA layer is a matrix  $\mathbf{X} \in \mathbb{R}^{N \times w}$  containing the history of length  $w$  of all nodes in the graph. We denote by  $\tilde{\mathbf{x}}$  the maximum of the input values over the time dimension,  $\tilde{\mathbf{x}}_i = \max_j \mathbf{X}_{i,j}$ . The gating operation produces matrix  $\mathbf{G} \in \mathbb{R}^{N \times Nw}$ . Row  $i$  of the gated matrix corresponds to node  $i$  and it contains all the information accumulated by the graph during past  $w$  steps:

$$\mathbf{G}_{i,j+k} = \text{ReLU}[(\mathbf{W}_{i,j} \mathbf{X}_{j,k} - \tilde{\mathbf{x}}_i) / \tilde{\mathbf{x}}_i]. \quad (2)$$

Graph gate relates the information collected by nodes  $i, j$  via two mechanisms. First, the information that is supposed to flow from node  $j$  to node  $i$  is gated by graph weights  $\mathbf{W}_{i,j}$ . Second, the values of node  $j$  are related to the max value of node  $i$ . Input scaling is popular in neural TS forecasting, often taking form  $\mathbf{X}_{j,k} / \tilde{\mathbf{x}}_j$ . In the multivariate context it may be important to preserve the information about the relative magnitude difference between nodes  $i$  and  $j$ . We observed empirically that a more standard scaling  $\mathbf{X}_{j,k} / \tilde{\mathbf{x}}_j$  in this scenario leads to significant loss of information.

**Fully connected time-series block:** We propose a fully connected residual architecture with  $L$  hidden layers,  $R$  residual blocks and weights shared across nodes. Its input for node  $i$ ,  $\mathbf{Z}_i$ , is conditioned on the node embedding and its own history:  $\mathbf{Z} = [\mathbf{E}, \mathbf{X} / \tilde{\mathbf{x}}, \mathbf{G}]^T$ ,  $\mathbf{Z} \in \mathbb{R}^{N(w+1)+d \times N}$ . Using residual block and layer superscripts and denoting the fully connected layer with weights  $\mathbf{A}^{r,\ell}$  and biases  $\mathbf{b}^{r,\ell}$  as

$\text{FC}_{r,\ell}(\mathbf{H}^{r,\ell-1}) \equiv \text{ReLU}(\mathbf{A}^{r,\ell}\mathbf{H}^{r,\ell-1} + \mathbf{b}^{r,\ell})$ , the operation of the fully connected residual TS modeling architecture is described as follows:

$$\begin{aligned}\mathbf{Z}^r &= \text{ReLU}[\mathbf{Z}^{r-1} - \widehat{\mathbf{Z}}^{r-1}], \\ \mathbf{H}^{r,1} &= \text{FC}_{r,1}(\mathbf{Z}^r), \dots, \mathbf{H}^{r,L} = \text{FC}_{r,L}(\mathbf{H}^{r,L-1}), \\ \widehat{\mathbf{Z}}^r &= \mathbf{B}^r \mathbf{H}^{r,L}, \widehat{\mathbf{Y}}^r = (\mathbf{H}^{r,L})^T \mathbf{F}^r.\end{aligned}\tag{3}$$

We assume  $\widehat{\mathbf{Z}}^0 \equiv \mathbf{0}$ ,  $\mathbf{Z}^0 \equiv \mathbf{Z}$ ; projection matrices have dimensions  $\mathbf{B}^r \in \mathbb{R}^{N(w+1)+d \times d_h}$ ,  $\mathbf{F}^r \in \mathbb{R}^{d_h \times H}$  and the final forecast is the sum of forecasts of all residual blocks,  $\widehat{\mathbf{Y}} = \sum_r \widehat{\mathbf{Y}}^r$ .

**FC-GAGA layer stacking:** FC-GAGA layer stacking methodology is based on the following three principles. First, the next layer accepts the sum of forecasts of previous layers as input. Second, each FC-GAGA layer has its own set of node embeddings and thus its own graph gate. Thus each layer is provided a freedom to gate the information flow across nodes in accordance with the processing already accomplished by the previous layer. For example, in the first FC-GAGA layer, for node id 5, it may be optimal to focus on the histories of node ids [10, 200, 500]. However, since the first FC-GAGA layer updates the states of all nodes, node 5 may no longer need the information provided by nodes [10, 200, 500], nor by their neighbours; and instead may wish to focus on node ids [3 and 15], as they now provide more important information. This is clearly a more flexible information diffusion model than the Markov model based on node proximity that is common in the traffic forecasting literature [17]. Finally, the final model output is equal to the average of forecasts produced by each FC-GAGA layer.

**Complexity analysis:** In the following analysis we skip the batch dimension and compute the complexity involved in creating a single forecast of length  $H$  for all nodes  $N$  in the graph when the input history is of length  $w$ , the node embedding width is  $d$  and the hidden layer width is  $d_h$ . Analysis details can be found in Appendix B. The graph gate block has complexity  $O(N^2(w+d))$ , as is evident from eq. (2). The time gate mechanism producing a seasonality factor for each node using its associated time feature scales linearly with the number of nodes, the hidden dimension, the input history length:  $O(N(d+w)d_h)$ . Finally, the fully-connected TS model with  $L$  FC layers and  $R$  residual blocks that accepts the flattened input  $N \times Nw$  has complexity  $O(R(2N^2wd_h + (L-2)Nd_h^2))$ . In most practical configurations, the total complexity of the model will be dominated by  $O(N^2Rwd_h)$ .

### 3 Empirical Results

**Datasets:** FC-GAGA is evaluated on two traffic datasets, METR-LA and PEMS-BAY [7, 17] consisting of the traffic speed readings collected from loop detectors and aggregated over 5 minute intervals. METR-LA contains 34,272 time steps of 207 sensors collected in Los Angeles County over 4 months. PEMS-BAY contains 52,116 time steps of 325 sensors collected in the Bay Area over 6 months. The datasets are split in 70% training, 10% validation, and 20% test, as defined in [17].

**Baselines:** We compare FC-GAGA both with temporal models that do not require a pre-specified graph and spatio-temporal models that may rely on a pre-specified graph or have a learnable graph as part of the model. The following univariate temporal models provided by [17] are considered: ARIMA [20], implemented using a Kalman filter; SVR [40], a linear Support Vector Regression model; FNN, a Feedforward Neural Network; and FC-LSTM [37], a sequence-to-sequence model that uses fully connected LSTMs in encoder and decoder. The spatio-temporal models include DCRNN [17] (Diffusion Convolutional Recurrent Neural Network, a graph convolutional network inside the sequence-to-sequence architecture); STGCN [43] (Spatio-Temporal Graph Convolutional Network, merges graph convolutions with gated temporal convolutions); Graph WaveNet [41], fuses graph convolution and dilated causal convolution; and GMAN [48] (Graph Multi-Attention Network, an encoder-decoder model with multiple spatio-temporal attention blocks, and a transform attention layer between the encoder and the decoder). Of these methods, only Graph Wavenet can generate predictions without a pre-specified graph. For DCRNN, STGCN, Graph WaveNet and GMAN and we use the settings an report results from the original papers.

**FC-GAGA architecture details and training setup:** Scalar  $\varepsilon$  in (1) is set to 10. The embedding dimensionality,  $d$ , is set to 64 and the hidden layer width  $d_h$  for all fully connected layers is set to 128. The number of layers  $L$  in the fully-connected TS model is equal to 3 and the number of blocks  $R$  is



Table 1: Error metrics computed using the standard protocol [41] (average over last time step of horizon, input window length 12). Lower numbers are better. <sup>‡</sup>Graph Wavenet trained using official code by the authors using only adaptive matrix without the support of geographical adjacency matrix.

Dataset	Models	15 min			30 min			60 min		
		MAE	MAPE	RMSE	MAE	MAPE	RMSE	MAE	MAPE	RMSE
METR-LA	DCRNN	2.77	7.30%	5.38	3.15	8.80%	6.45	3.60	10.50%	7.60
	STGCN	2.88	7.62%	5.74	3.47	9.57%	7.24	4.59	12.70%	9.40
	Graph WaveNet	2.69	6.90%	5.15	3.07	8.37%	6.22	3.53	10.01%	7.37
	GMAN	2.77	7.25%	5.48	3.07	8.35%	6.34	3.40	9.72%	7.21
	ARIMA	3.99	9.60%	8.21	5.15	12.70%	10.45	6.90	17.40%	13.23
	SVR	3.99	9.30%	8.45	5.05	12.10%	10.87	6.72	16.70%	13.76
	FNN	3.99	9.90%	7.94	4.23	12.90%	8.17	4.49	14.00%	8.69
	FC-LSTM	3.44	9.60%	6.30	3.77	10.90%	7.23	4.37	13.20%	8.69
	Graph WaveNet <sup>‡</sup>	2.80	7.45%	5.45	3.18	9.00%	6.42	3.57	10.47%	<b>7.29</b>
	FC-GAGA	<b>2.75</b>	<b>7.25%</b>	<b>5.34</b>	<b>3.10</b>	<b>8.57%</b>	<b>6.30</b>	<b>3.51</b>	<b>10.14%</b>	7.31
PEMS-BAY	DCRNN	1.38	2.90%	2.95	1.74	3.90%	3.97	2.07	4.90%	4.74
	STGCN	1.36	2.90%	2.96	1.81	4.17%	4.27	2.49	5.79%	5.69
	Graph WaveNet	1.30	2.73%	2.74	1.63	3.67%	3.70	1.95	4.63%	4.52
	GMAN	1.34	2.81%	2.82	1.62	3.63%	3.72	1.86	4.31%	4.32
	ARIMA	1.62	3.50%	3.30	2.33	5.40%	4.76	3.38	8.30%	6.50
	SVR	1.85	3.80%	3.59	2.48	5.50%	5.18	3.28	8.00%	7.08
	FNN	2.20	5.19%	4.42	2.30	5.43%	4.63	2.46	5.89%	4.98
	FC-LSTM	2.05	4.80%	4.19	2.20	5.20%	4.55	2.37	5.70%	4.96
	Graph WaveNet <sup>‡</sup>	<b>1.34</b>	<b>2.79%</b>	<b>2.83</b>	1.69	<b>3.79%</b>	<b>3.80</b>	2.00	4.73%	4.54
	FC-GAGA	1.36	2.87%	2.86	<b>1.68</b>	3.80%	<b>3.80</b>	<b>1.97</b>	<b>4.67%</b>	<b>4.52</b>

equal to 2. We use weight decay of  $1e-5$  to regularize fully-connected layers. The model is trained using the Adam optimizer with default tensorflow settings and initial learning rate of 0.001 for 60 epochs. The learning rate is annealed by a factor of 2 every 6 epochs starting at epoch 43. One epoch consists of 800 batches of size 4 and the model takes the history of 12 points and predicts 12 points (60 min) ahead in one shot. Each training batch is assembled using 4 time points chosen uniformly at random from the training set and the histories of all nodes collected at each of the time points. As METR-LA has 207 sensor nodes and in PEMS-BAY has 325 sensor nodes, this results in the batches consisting of  $207 \cdot 4 = 828$  and  $325 \cdot 4 = 1300$  time-series, respectively. The objective function used to train the network is MAE, averaged over all nodes and all forecasts within horizon  $H = 12$ :

$$\mathcal{L} = \frac{1}{HN} \sum_{i=1}^H \sum_{v=1}^N |y_{v,T+i} - \hat{y}_{v,T+i}|. \quad (4)$$

**Quantitative results:** Our key empirical results appear in Table 1. FC-GAGA compares favourably even against graph-based models that rely on additional external graph definitions on both METR-LA and PEMS-BAY datasets (DCRNN, STGCN, Graph WaveNet, and GMAN). Most of the time, FC-GAGA outperforms Graph WaveNet model when they are trained and evaluated in the same conditions, i.e. both models only rely on the graph learned from the data (Graph WaveNet is using only the *adaptive* adjacency matrix that it learns from the data). It significantly outperforms the univariate models not using any graphical models internally (ARIMA, SVR, FNN, and FC-LSTM).

**Qualitative results:** The final FC-GAGA forecast is composed of the average of the forecasts of individual layers. Figure 2 shows the contributions of different layers to the final 15 min ahead forecast (after scaling by the averaging factor  $1/3$ ). We can see that the role of the first layer is mostly to provide a baseline forecast, while at the same time accounting for some of the seasonal effects. The layer 2 contribution to the prediction clearly captures a daily seasonality effect. Layer 2 and especially layer 3 provide iterative correction terms to the original baseline produced by layer 1, based on the most recent data. This is especially evident for layer 3 whose output is inactive most of the time, becoming active when significant correction is required because the observed signals undergo significant stochastic changes in short periods of time.

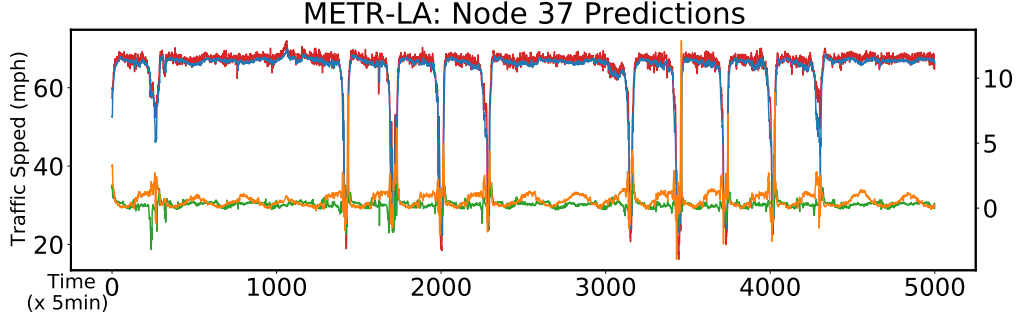


Figure 2: FC-GAGA 15 min ahead forecasts for node 37 in METR-LA dataset. Blue, green and orange lines depict the partial forecasts produced by layers 1, 2, and 3 of the architecture respectively. Blue & red: left axis; orange & green: right axis. Additional results appear in Appendix A.

Next, we show in Fig. 3 the geographical distribution of the weights  $\mathbf{W}_{i,j}$  in the graph gate, specified in eq. (2), for layers 1–3, as learned for the METR-LA dataset. Each layer is provided the freedom to learn its own relationship across graph nodes; the learned relationships differ significantly across layers, indicating information aggregation from different spatial regions. In Fig. 4 (left) we observe that the gating is less strictly enforced in the first layer (the average  $\mathbf{W}_{i,j}$  values are higher in the first layer) and the geographic distribution of values is more dispersed (see Fig. 3, left). We interpret this as indicating that in layer 1 FC-GAGA collects information across a wide variety of nodes and geographical locations to construct a stable baseline forecast. As we move from layer 2 to layer 3, we can see that the nodes with highest graph weights more tightly concentrate around the target node for which the forecast is produced (see Fig. 3, middle and right and Fig. 4, right). Fig. 4 (left) indicates that many more  $\mathbf{W}_{i,j}$  have smaller values progressively in layers 2 and 3, implying stricter gating in eq. (2). Our interpretation of this is that to provide iterative updates to the baseline forecast, FC-GAGA focuses on the nodes that are closer to the target node and restricts the information flow such that the correction terms are defined by the nodes with the most relevant information.

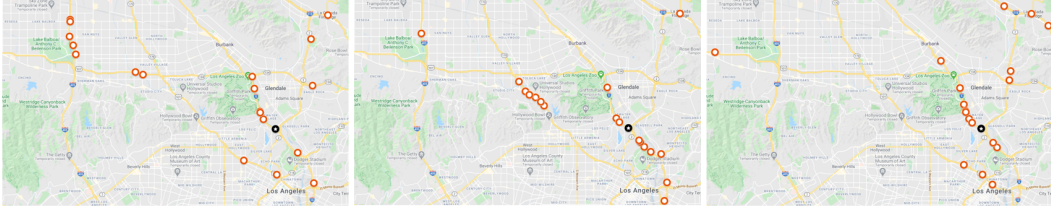


Figure 3: Maps of 20 highest weighted nodes for layers 1, 2, and 3. Black star is the forecasted node.

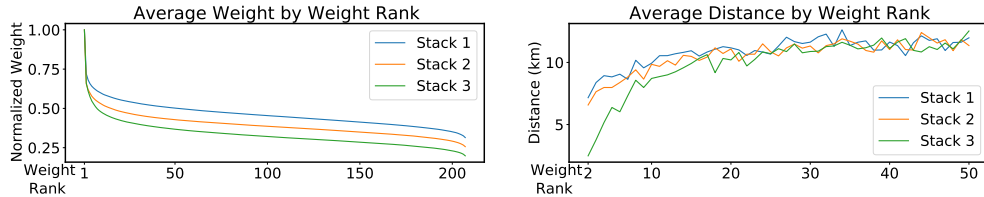


Figure 4: Average of graph gate weights  $\mathbf{W}_{i,j}$  normalized by the self-weight  $\mathbf{W}_{i,i}$  (left) and their average distances from the forecasted node (right) per FC-GAGA layer in METR-LA dataset.

**Ablation studies:** Our ablation studies validate (i) the effectiveness of the FC-GAGA layer stacking mechanism, and (ii) the effectiveness of the graph gating mechanism proposed in eq. (2). Table 2 demonstrates the performance of FC-GAGA on the METR-LA and PEMS-BAY datasets as a function

Table 2: Ablation study: the effectiveness of the FC-GAGA layer stacking

Dataset	Layers	15 min			30 min			60 min		
		MAE	MAPE	RMSE	MAE	MAPE	RMSE	MAE	MAPE	RMSE
METR-LA	1	2.80	7.36%	5.44	3.17	8.82%	6.44	3.63	10.55%	7.48
	2	2.77	7.30%	5.37	3.13	8.74%	6.39	3.54	10.41%	7.36
	3	2.75	7.25%	5.34	3.10	8.57%	6.30	3.51	10.14%	7.31
	4	2.75	7.21%	5.34	3.10	8.54%	6.34	3.52	10.19%	7.34
PEMS-BAY	1	1.35	2.85%	2.85	1.69	3.85%	3.83	2.00	4.78%	4.61
	2	1.36	2.87%	2.86	1.68	3.80%	3.81	1.97	4.64%	4.52
	3	1.36	2.87%	2.86	1.68	3.80%	3.80	1.97	4.67%	4.52
	4	1.35	2.83%	2.86	1.69	3.78%	3.83	1.98	4.66%	4.57

Table 3: Ablation study: the effectiveness of the FC-GAGA graph gate block proposed in eq. (2)

Dataset	Graph gate $\mathbf{W}$	Layers	15 min			30 min			60 min		
			MAE	MAPE	RMSE	MAE	MAPE	RMSE	MAE	MAPE	RMSE
METR-LA	learnable	3	2.75	7.15%	5.31	3.09	8.44%	6.28	3.51	10.06%	7.25
	ones	3	2.87	7.71%	5.67	3.24	9.22%	6.71	3.67	10.80%	7.65
	zeros	3	2.97	7.80%	5.87	3.54	9.88%	7.25	4.35	12.77%	8.93
PEMS-BAY	learnable	3	1.36	2.87%	2.86	1.69	3.80%	3.81	1.97	4.65%	4.52
	ones	3	1.38	2.89%	2.89	1.70	3.82%	3.86	2.00	4.70%	4.60
	zeros	3	1.41	2.92%	3.05	1.86	4.10%	4.27	2.44	5.58%	5.66

of the number of the FC-GAGA layers. We can see that increasing the number of layers leads to substantial improvement on the METR-LA dataset, while on PEMS-BAY the number of layers does not affect performance metrics significantly. METR-LA is known to be a harder problem than PEMS-BAY because of the more erratic nature of its TS. This implies that increasing the number of FC-GAGA layers to solve harder problems may bring additional accuracy benefits while using only one FC-GAGA layer to solve an easier problem may be beneficial from the computational efficiency standpoint (the runtime scales approximately linearly with the number of layers). Table 3 shows the results of ablating the graph gate mechanism described in eq. (2) with a 3-layer FC-GAGA network. We can see that the proposed version with learnable graph gate weights  $\mathbf{W} = \exp(\epsilon \mathbf{E} \mathbf{E}^T)$  performs best, confirming its effectiveness. We also test the version with  $\mathbf{W}$  set to all zeros, which amounts to always closing the gate, in which case FC-GAGA is running in the univariate regime, only having access to the history of the target node when forecasting. We can see that this results in a very strong univariate baseline, outperforming all univariate methods in Table 1 (ARIMA, SVR, FNN, FC-LSTM) by a large margin. In the case when  $\mathbf{W}$  is set to all ones, FC-GAGA is clearly provided with more information from the other graph nodes, which results in improved performance, which is clearly sub-optimal when  $\mathbf{W}$  is not learned.

**Profiling results:** To confirm FC-GAGA’s computational efficiency we conducted a profiling experiment using a P100 GPU in the default Google Colab environment. We profiled the original codes provided by the authors of DCRNN [17] and Graph Wavenet [41]. We profiled our tensorflow 2.0 implementation of FC-GAGA, which only relies on standard Keras layer definitions, with no attempt to optimize for memory or speed. We can clearly see that FC-GAGA is more computationally effective as it consumes approximately half the memory and compute time of Graph WaveNet and it is about 10 times faster than DCRNN and about 5-10 times more memory efficient. We can also see that it scales well between METR-LA (207 nodes) and PEMS-BAY (325 nodes) datasets, which may be an important property for handling larger scale problems with thousands of nodes.

## 4 Related Work

Multivariate TS prediction or forecasting has been studied intensively for decades. Approaches based on statistical models include the vector autoregressive (VAR) and VAR moving average (VARMA) models [5]. Sparse VAR models can perform better; these often incorporate inference of a causal

Table 4: Profiling results: total training and evaluation runtime, and GPU memory utilization. Measured using official DCRNN and Graph WaveNet codes and our non-optimized tensorflow implementation of FC-GAGA on NVIDIA P100 GPU in the default Google Colab environment.

Models	METR-LA		PEMS-BAY	
	Runtime, min	GPU memory, GB	Runtime, min	GPU memory, GB
DCRNN	358	8.63	828	8.63
Graph WaveNet	90	2.14	192	2.75
FC-GAGA	37	0.93	69	1.47

graphical model to capture the relationships between the different variables [1, 4, 21, 36]. The linearity of these models can impede forecasting accuracy, so kernel versions have been introduced [18, 31]; a similar approach in [38] trains separate MLPs (or RNNs or LSTMs) for each output TS. Historically, neural network approaches have struggled to compete in terms of prediction accuracy with state-of-the-art statistical forecasting models, such as Prophet [39]. This has changed over the past few years. Several neural network architectures that are trained on many time series, but then form predictions for a single variable based on its past history (and covariates) have eclipsed statistical methods [24, 27, 29, 34]. In contrast to our work, these architectures do not simultaneously form forecasts for multiple time series using past information from all of them. Other methods use multiple input time-series to predict a single target TS [3, 6, 11, 14, 26]. It is conceivable to train multiple such architectures to perform inference of multiple target time series. For these architectures, several innovations have proven effective, including attention mechanisms to determine which input variables and time lags to focus on [11, 19, 22, 26]. In this vein, the transformer architecture is modified in [16] to address TS forecasting and DeepGLO [30] is a hybrid model that combines regularized matrix factorization to derive factors with a temporal convolution network for local prediction.

**Graph-based models:** In some settings, we are provided with a graph that is thought to capture the relationships between the variables. There has been an intensive research effort to derive architectures that can use this graph information to perform improved forecasting. The graph VAR/VARMA proposed in [13] is a linear model with coefficients specified in terms of the graph Laplacian. The neural network architectures usually combine graph convolutional networks (GCNs), which can focus on spatial relationships, with GRUs, LSTMs, TCNs, or RNNs [8, 12, 17, 43, 47]. A few approaches apply graph-based learning directly to a spatio-temporal graph [35, 44]. Performance can be improved using attention mechanisms [2, 10, 25, 32, 48]. More advanced architectures also offer an avenue for improvement. ST-UNet [45] employs spatio-temporal pooling/unpooling to allow the architecture to learn representations at multiple scales. Graph WaveNet [41] employs dilated causal convolution to extract temporal relationships from a larger perceptive field. Xu et al. [42] introduce spatial-temporal transformer networks.

The graphs are often derived from considerations that do not correspond exactly to the prediction task. For example, a graph for traffic forecasting might be based on geographical proximity rather than road network connectivity. It can be beneficial to learn an appropriate graph from the data. The algorithms in [9, 44] learn the graph as a pre-processing step. A better approach is to combine graph learning with prediction; the architectures in [41, 46] incorporate mechanisms to learn adaptive adjacency matrices that are subsequently used in GCNs.

## 5 Conclusions

We proposed and empirically validated a novel neural architecture for spatio-temporal forecasting, which we call FC-GAGA (Fully Connected Gated Graph Architecture). FC-GAGA combines a fully connected TS model with temporal and graph gating mechanisms, that are both generally applicable and computationally efficient. We empirically demonstrate that the proposed general model can be learned efficiently from the data to capture non-Markovian relations across multiple variables over layers in the architecture, resulting in excellent generalization performance. We further profile FC-GAGA’s training and inference runtime and demonstrate that it is several times more efficient in the utilization of GPU memory and compute than existing models with comparable accuracy. Our results provide compelling positive evidence to stimulate the development of fully connected architectures for graph based information processing.

## Broader Impact

Forecasting is among the oldest problems tackled by the human civilization [23]. Additionally, it can be broadly related to self-supervised learning, also known as filling in the blanks, which is often considered the foundation of common sense and intelligent behaviour [15]. Strictly speaking, any control system involves forecasting in one disguise or another as part of the control loop. Therefore, improved forecasting algorithms have the potential to profoundly impact a wide array of fields in which planning and intelligent decision making are essential.

One of the contributions of the current work is that the proposed approach is significantly more computationally efficient compared to existing alternatives. This is an important factor in democratizing the use and acceptance of advanced AI algorithms, which can be appreciated at different levels. It is important to work towards closing the gap between large organizations with unlimited compute and small businesses and startups that may not have enough budget to run a GPU cluster or buy expensive compute from larger organizations. In the same spirit, but more broadly speaking, it is even more important to provide opportunities for poor countries and regions to use advanced AI technologies even if their compute capabilities are limited. Improving the computational efficiency of AI algorithms while maintaining their accuracy is an important step in this direction.

In this paper we address a particular type of forecasting problem, which involves simultaneously forecasting multiple time series originating from entities related via an unknown underlying graph. As an application domain example, we focus on forecasting road traffic, using a collection of sensors mounted on highways. This has obvious applications in traffic management, and can have immediate positive effects through reducing  $CO_2$  emissions as well as improving the quality of life of the general population commuting to and from work every day. However, a much broader variety of problems can be cast in this formulation. Examples include weather forecasting and electrical grid load forecasting. Weather forecasting relies on an array of geographically spread weather stations. The weather observations obtained by a collection of weather stations can obviously be modelled using a spatio-temporal graph with nodes related via underlying dependent weather fluctuations. Accurate weather forecasts are important to support many aspects of smart agriculture including timely water supply in water deprived areas. Another important potential application of our method is the integration of solar energy in the regular energy grid, where accurately forecasting short-term load, long-term demand and the viable solar energy supply are critical to make sure that the integration of solar energy is economically viable and safe [28]. It is clear that tackling the weather forecasting problem can have long ranging impact on alleviating food supply issues and starvation, whereas tackling the solar energy integration problem will have long ranging impact on making the world economy more sustainable and will help to fight climate change.

In this paper, in terms of the application domain, we focus on the spatio-temporal forecasting of traffic. The wider impact of our work is clear even with this particular focus in mind. The methods we develop are general and hence it is reasonable to expect that they will be applicable in additional fields, including those we identified above, i.e., weather forecasting, smart agriculture and solar energy integration. For the moment, we have not conducted empirical studies in these domains, which is a clear limitation of the current study, one that we are excited to address in our future work. Additionally, although the current study does rely on a solid empirical investigation based on two real-life datasets, it is still limited in coverage and our future effort will focus on increasing the number of datasets that are used for empirical investigation. Finally, machine learning based time series forecasting models are affected by the problems of overfitting and distribution shift, perhaps as much as other machine learning algorithms. The time series forecasting problem brings about additional challenges such as structural breaks, when one abrupt event globally affects the distribution of data for an arbitrary duration of time, rendering a part, or even the whole history, of the training data invalid, and often breaking the existing model or model training pipeline. Measures to recognize and rectify the effects of such events are very important to implement to make sure that the use of advanced AI models, such as ours, is safe and profitable.

## References

- [1] F. R. Bach and M. I. Jordan. Learning graphical models for stationary time series. *IEEE Trans. Signal Processing*, 52(8):2189–2199, 2004.
- [2] L. Bai, L. Yao, S. Kanhere, X. Wang, and Q. Sheng. STG2Seq: Spatial-temporal graph to sequence model for multi-step passenger demand forecasting. In *Proc. Int. Joint Conf. Artificial Intelligence*, pages 1981–1987, 2019.
- [3] W. Bao, J. Yue, and Y. Rao. A deep learning framework for financial time series using stacked autoencoders and long-short term memory. *PloS One*, 12(7), 2017.
- [4] A. Bolstad, B. D. Van Veen, and R. Nowak. Causal network inference via group sparse regularization. *IEEE Trans. Signal Processing*, 59(6):2628–2641, 2011.
- [5] G. E. Box, G. M. Jenkins, G. C. Reinsel, and G. M. Ljung. *Time series analysis: forecasting and control*. John Wiley & Sons, 2015.
- [6] Y.-Y. Chang, F.-Y. Sun, Y.-H. Wu, and S.-D. Lin. A memory-network based solution for multivariate time-series forecasting. *arXiv preprint arXiv:1809.02105*, 2018.
- [7] C. Chen, K. Petty, A. Skabardonis, P. Varaiya, and Z. Jia. Freeway performance measurement system: Mining loop detector data. *Transportation Research Record*, 1748(1):96–102, 2001.
- [8] C. Chen, K. Li, S. G. Teo, X. Zou, K. Wang, J. Wang, and Z. Zeng. Gated residual recurrent graph neural networks for traffic prediction. In *Proc. AAAI Conf. Artificial Intelligence*, pages 485–492, 2019.
- [9] Z. Diao, G. Wang, D. Zhang, Y. Liu, K. Xie, and S. He. Dynamic spatial-temporal graph convolutional neural networks for traffic forecasting. In *Proc. AAAI Conf. Artificial Intelligence*, 2019.
- [10] S. Guo, Y. Lin, N. Feng, C. Song, and H. Wan. Attention based spatial-temporal graph convolutional networks for traffic flow forecasting. In *Proc. AAAI Conf. Artificial Intelligence*, volume 33, pages 922–929, 2019.
- [11] T. Guo and T. Lin. Multi-variable LSTM neural network for autoregressive exogenous model. *arXiv preprint arXiv:1806.06384*, 2018.
- [12] Y. Huang, Y. Weng, S. Yu, and X. Chen. Diffusion convolutional recurrent neural network with rank influence learning for traffic forecasting. In *Proc. IEEE Int. Conf. Big Data Science And Engineering*, pages 678–685, Aug 2019.
- [13] E. Isufi, A. Loukas, N. Perraudin, and G. Leus. Forecasting time series with VARMA recursions on graphs. *IEEE Trans. Sig. Process.*, 67(18):4870–4885, Sept. 2019.
- [14] G. Lai, W.-C. Chang, Y. Yang, and H. Liu. Modeling long-and short-term temporal patterns with deep neural networks. In *Proc. ACM Int. Conf. Research & Development in Information Retrieval*, pages 95–104, 2018.
- [15] Y. LeCun. Deep learning hardware: Past, present, and future. In *2019 IEEE International Solid-State Circuits Conference - (ISSCC)*, pages 12–19, 2019.
- [16] S. Li, X. Jin, Y. Xuan, X. Zhou, W. Chen, Y.-X. Wang, and X. Yan. Enhancing the locality and breaking the memory bottleneck of transformer on time series forecasting. In *Advances in Neural Information Processing Systems*, pages 5244–5254, 2019.
- [17] Y. Li, R. Yu, C. Shahabi, and Y. Liu. Diffusion convolutional recurrent neural network: Data-driven traffic forecasting. In *Proc. Int. Conf. Learning Representations*, 2018.
- [18] N. Lim, F. d’Alché Buc, C. Auliac, and G. Michailidis. Operator-valued kernel-based vector autoregressive models for network inference. *Machine Learning*, 99(3):489–513, 2015.
- [19] F. Liu, Y. Lu, and M. Cai. A hybrid method with adaptive sub-series clustering and attention-based stacked residual LSTMs for multivariate time series forecasting. *IEEE Access*, 8:62423–62438, 2020.
- [20] S. Makridakis and M. Hibon. ARMA models and the Box–Jenkins methodology. *Journal of Forecasting*, 16(3):147–163, 1997.
- [21] J. Mei and J. M. Moura. Signal processing on graphs: Causal modeling of unstructured data. *IEEE Trans. Signal Processing*, 65(8):2077–2092, 2016.

- [22] L. Munkhdalai, T. Munkhdalai, K. H. Park, T. Amarbayasgalan, E. Erdenebaatar, H. W. Park, and K. H. Ryu. An end-to-end adaptive input selection with dynamic weights for forecasting multivariate time series. *IEEE Access*, 7:99099–99114, 2019.
- [23] A. A. Neale. Weather forecasting: Magic, art, science and hypnosis. *Weather and Climate*, 5(1): 2–5, 1985.
- [24] B. N. Oreshkin, D. Carpo, N. Chapados, and Y. Bengio. N-BEATS: Neural basis expansion analysis for interpretable time series forecasting. In *Proc. Int. Conf. Learning Representations*, 2020.
- [25] C. Park, C. Lee, H. Bahng, T. Won, K. Kim, S. Jin, S. Ko, and J. Choo. STGRAT: A spatio-temporal graph attention network for traffic forecasting. *arXiv preprint arXiv:1911.13181*, 2019.
- [26] Y. Qin, D. Song, H. Chen, W. Cheng, G. Jiang, and G. W. Cottrell. A dual-stage attention-based recurrent neural network for time series prediction. In *Proc. Int. Joint Conf. Artificial Intelligence*, 2017.
- [27] S. S. Rangapuram, M. W. Seeger, J. Gasthaus, L. Stella, Y. Wang, and T. Januschowski. Deep state space models for time series forecasting. In *Advances in Neural Information Processing Systems*, pages 7785–7794, 2018.
- [28] D. Rolnick, P. L. Donti, L. H. Kaack, K. Kochanski, A. Lacoste, K. Sankaran, A. S. Ross, N. Milojevic-Dupont, N. Jaques, A. Waldman-Brown, A. Luccioni, T. Maharaj, E. D. Sherwin, S. K. Mukkavilli, K. P. Körding, C. Gomes, A. Y. Ng, D. Hassabis, J. C. Platt, F. Creutzig, J. Chayes, and Y. Bengio. Tackling climate change with machine learning. *CoRR*, abs/1906.05433, 2019.
- [29] D. Salinas, V. Flunkert, J. Gasthaus, and T. Januschowski. DeepAR: Probabilistic forecasting with autoregressive recurrent networks. *Int. J. Forecasting*, 2019.
- [30] R. Sen, H.-F. Yu, and I. S. Dhillon. Think globally, act locally: A deep neural network approach to high-dimensional time series forecasting. In *Adv. Neural Information Processing Systems*, pages 4838–4847, 2019.
- [31] Y. Shen, G. B. Giannakis, and B. Baingana. Nonlinear structural vector autoregressive models with application to directed brain networks. *IEEE Trans. Signal Processing*, 67(20):5325–5339, 2019.
- [32] X. Shi, H. Qi, Y. Shen, G. Wu, and B. Yin. A spatial-temporal attention approach for traffic prediction. *IEEE Trans. Intelligent Transportation Systems*, pages 1–10, Apr. 2020.
- [33] P. K. Singh, Y. Gupta, N. Jha, and A. Rajan. Fashion retail: Forecasting demand for new items. *CoRR*, abs/1907.01960, 2019.
- [34] S. Smyl. A hybrid method of exponential smoothing and recurrent neural networks for time series forecasting. *International Journal of Forecasting*, 36(1):75 – 85, 2020.
- [35] C. Song, Y. Lin, S. Guo, and H. Wan. Spatial-temporal synchronous graph convolutional networks: A new framework for spatial-temporal network data forecasting. In *Proc. AAAI Conf. Artificial Intelligence*, 2020.
- [36] J. Songsiri and L. Vandenberghe. Topology selection in graphical models of autoregressive processes. *Journal of Machine Learning Research*, 11(Oct):2671–2705, 2010.
- [37] I. Sutskever, O. Vinyals, and Q. V. Le. Sequence to sequence learning with neural networks. In *Adv. Neural Information Processing Systems*, pages 3104–3112, 2014.
- [38] A. Tank, I. Covert, N. Foti, A. Shojaie, and E. Fox. Neural Granger causality for nonlinear time series. *arXiv preprint arXiv:1802.05842*, 2018.
- [39] S. J. Taylor and B. Letham. Forecasting at scale. *The American Statistician*, 72(1):37–45, 2018.
- [40] C.-H. Wu, J.-M. Ho, and D. T. Lee. Travel-time prediction with support vector regression. *IEEE Trans. Intelligent Transportation Systems*, 5(4):276–281, 2004.
- [41] Z. Wu, S. Pan, G. Long, J. Jiang, and C. Zhang. Graph wavenet for deep spatial-temporal graph modeling. In *Proc. Int. Joint Conf. Artificial Intelligence*, pages 1907–1913, 2019.
- [42] M. Xu, W. Dai, C. Liu, X. Gao, W. Lin, G.-J. Qi, and H. Xiong. Spatial-temporal transformer networks for traffic flow forecasting. *arXiv preprint arXiv:2001.02908*, 2020.

- [43] B. Yu, H. Yin, and Z. Zhu. Spatio-temporal graph convolutional networks: A deep learning framework for traffic forecasting. In *Proc. Int. Joint Conf. Artificial Intelligence*, 2018.
- [44] B. Yu, M. Li, J. Zhang, and Z. Zhu. 3d graph convolutional networks with temporal graphs: A spatial information free framework for traffic forecasting. *arXiv preprint arXiv:1903.00919*, 2019.
- [45] B. Yu, H. Yin, and Z. Zhu. ST-UNet: A spatio-temporal U-network for graph-structured time series modeling. *arXiv e-prints, arXiv:1903.05631*, Mar. 2019.
- [46] Q. Zhang, J. Chang, G. Meng, S. Xiang, and C. Pan. Spatio-temporal graph structure learning for traffic forecasting. In *Proc. AAAI Int. Conf. Artificial Intelligence*, 2020.
- [47] L. Zhao, Y. Song, C. Zhang, Y. Liu, P. Wang, T. Lin, M. Deng, and H. Li. T-GCN: A temporal graph convolutional network for traffic prediction. *IEEE Trans. Intelligent Transportation Systems*, 2019.
- [48] C. Zheng, X. Fan, C. Wang, and J. Qi. GMAN: A graph multi-attention network for traffic prediction. In *Proc. AAAI Int. Conf. Artificial Intelligence*, 2020.



## A Dataset Details

FC-GAGA is evaluated on two traffic datasets, METR-LA and PEMS-BAY [7, 17]. METR-LA consists of the data of 207 sensors collected from loop detectors in the highway of Los Angeles County for 4 months from March 1st, 2012 to June 30th, 2012, i.e., 34,272 time steps. PEMS-BAY contains the data of 325 sensors in the Bay Area for 6 months from January 1st, 2017 to May 31th, 2017, i.e., 52,116 time steps. In both datasets, the traffic speed readings of sensors are aggregated into 5 minute windows. The datasets are split as 70% of data for training, 10% for validation, and 20% for testing, as originally defined in [17].

## B Complexity Analysis Details

In the following analysis we skip the batch dimension and compute the complexity involved in creating a single forecast of length  $H$  for all nodes  $N$  in the graph when the input history is of length  $w$ , the node embedding width is  $d$  and the hidden layer width is  $d_h$ . The graph gate block has complexity  $O(N^2(w + d))$ , as is evident from eq. (2), which involves the node interaction matrix  $N \times N$  derived from the  $N \times d$  embedding matrix and gating of the  $N^2w$  input values. The time gate mechanism produces a seasonality factor for each node using its associated time feature, so its complexity scales linearly with the number of nodes, the hidden dimension, the input history length and the forecast horizon, i.e.,  $O(N(d + w)d_h + NHd_h)$ . In most practical situations we have  $d + w > H$ . Finally, the fully-connected TS model with  $L$  FC layers and  $R$  residual blocks that accepts the flattened  $N \times Nw$  output of the graph gate scales as follows. The first and the last layers of the residual block scale as  $O(N^2wd_h)$  (recall that the last linear layer is doing a backcast from  $d_h$  to  $Nw$ ). The hidden layers scale as  $O(Nd_h^2)$ . This results in the total fully-connected TS model complexity  $O(R(2N^2wd_h + (L - 2)Nd_h^2))$ . In most practical configurations, the total complexity of the model will be dominated by  $O(N^2Rwd_h)$ .

## C Empirical Results Details

In this Appendix, we include some additional figures that provide further illustration of the behaviour of FC-GAGA.

**Stack contributions:** Figures 5 and 6 provide examples of how the different stacks in the architecture contribute to the prediction for the METR-LA and PEMS-BAY datasets, respectively. Figures 7 and 8 show the same information, but focus on shorter time windows.

As with the example provided in the main paper, we see that the first stack provides a (relatively accurate) baseline prediction in all cases, and then stacks 2 and 3 provide modifications to enhance the accuracy. Often these stacks provide a very small contribution; they become much more active when there are major changes in the signal (primarily during rush-hour on weekdays). For these periods, the stack 1 prediction struggles to provide the same level of accuracy after an abrupt change and stacks 2 and 3 can compensate. For several of the nodes (e.g., METR-LA node 124, PEMS-BAY nodes 30 and 179), we can see that stack 2 is responsibly for modeling a daily periodic fluctuation).

In Figures 7 and 8, we see clearer evidence of the compensation effect of stacks 2 and 3. For example, for node 31 in the METR-LA dataset, we see in Fig. 7 that the stack 1 prediction lags behind the true signal after the sudden drop, and struggles to return to the same level for close to an hour. Stack 2 (orange) compensates for this by providing a significant positive component to the prediction only during this period when the stack 1 prediction is trying to recover. For PEMS-BAY node 182 in Figure 8 it is clear that stacks 2 and 3 are compensating for the prediction lag of stack 1 whenever there are significant changes in the true signal.

**Spatial distribution of weights:** Figures 9- 15 display maps that show where the largest weights are for predictions of various nodes. As discussed in the main paper, we observe that different stacks obtain information from different spatial regions. There are usually fewer nodes with significant weight for the third stack and they tend to be located closer to the forecasted node (see the maps of the four largest weights).

**Weights for each stack:** Figure 16 depicts the average weight by weight rank (i.e., for the largest weight, what is the average value, etc.) for the PEMS-BAY dataset. The left panel of the figure shows clearly that the weights for stack 1 are higher than those of stack 2, which are in turn higher than stack 3. This illustrates how stack 1 incorporates information from many nodes in order to form its prediction, whereas stacks 2 and 3 use far fewer nodes (the weight gating blocks the contribution from many nodes). In the right panel of Figure 16, we show the average distance from the forecasted nodes for each weight rank. The results have similarities with those presented in the main paper for the METR-LA dataset, but there are also difference. As for the METR-LA dataset, the average distance increases with the weight rank, especially for stacks 1 and 3, and particularly for the first 20 ranks. For the PEMS-BAY dataset, we see that the distance for stack 2 does not grow as rapidly. This suggests that for PEMS-BAY stack 2 often incorporates information from nodes that are further away.

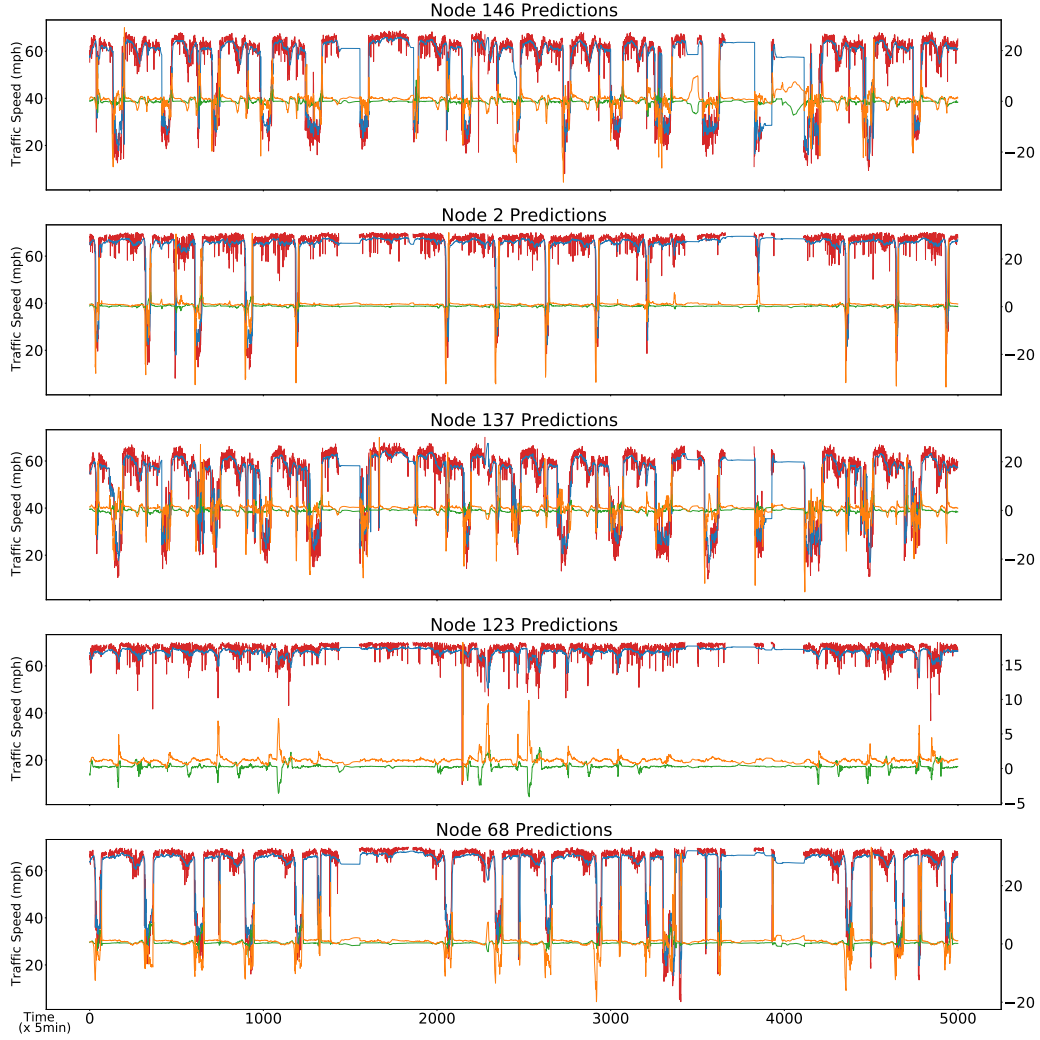


Figure 5: FC-GAGA 15 min ahead forecasts for different nodes in METR-LA dataset. Blue, green and orange lines depict the partial forecasts produced by layers 1, 2, and 3 of the architecture respectively. Magnitudes of blue and red lines are indicated by the left axis labels; magnitudes of orange and green lines are indicated by the right axis labels.

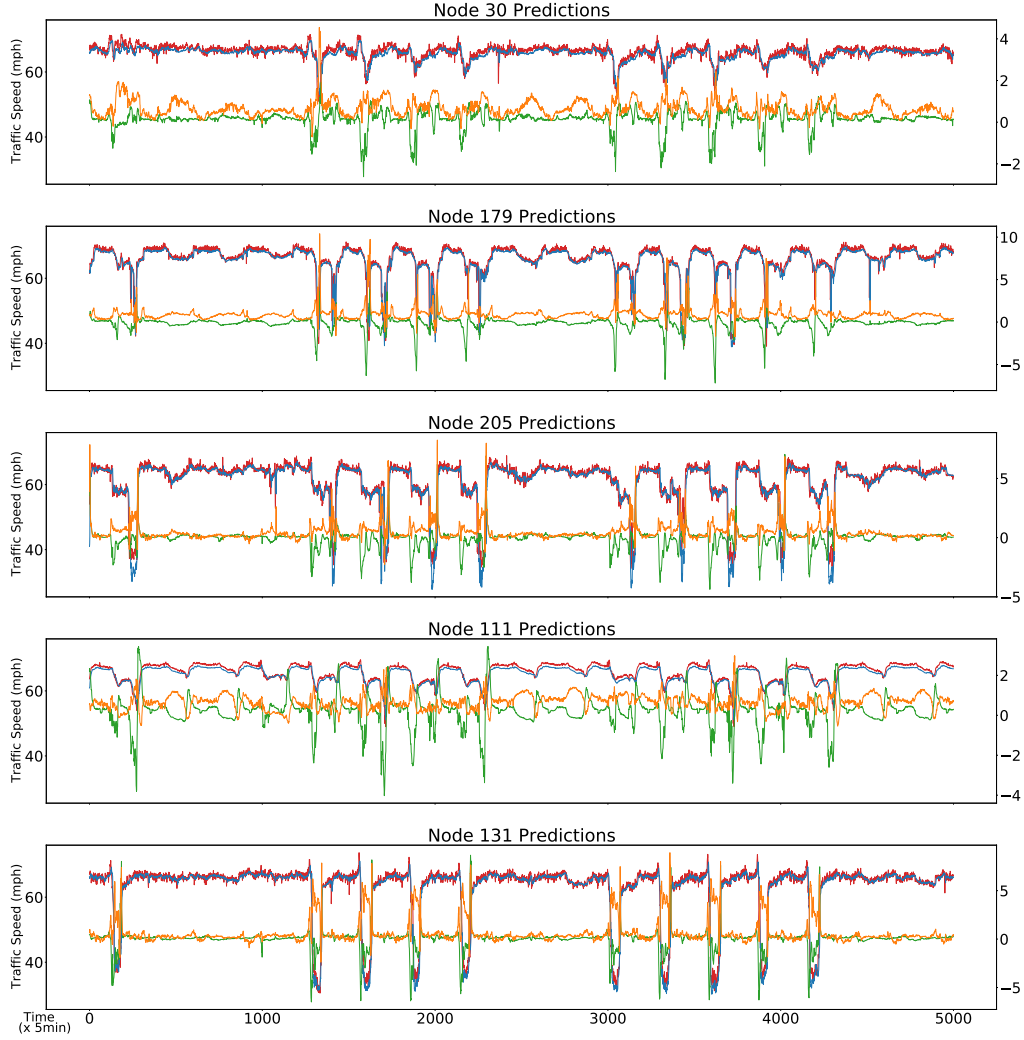


Figure 6: FC-GAGA 15 min ahead forecasts for different nodes in PEMS-BAY dataset. Blue, green and orange lines depict the partial forecasts produced by layers 1, 2, and 3 of the architecture respectively. Magnitudes of blue and red lines are indicated by the left axis labels; magnitudes of orange and green lines are indicated by the right axis labels.

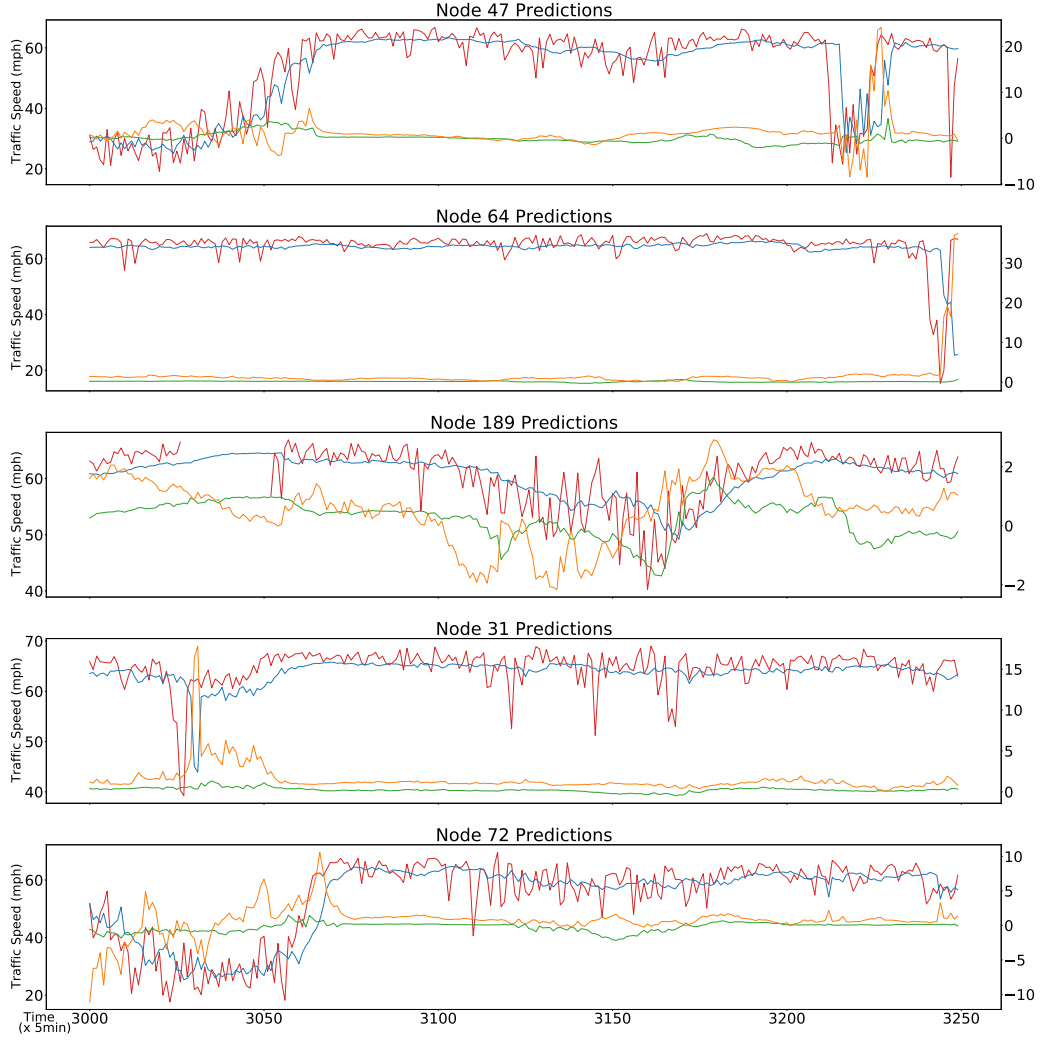


Figure 7: FC-GAGA 15 min ahead forecasts for different nodes in METR-LA dataset from time 3000 to 3250. Blue, green and orange lines depict the partial forecasts produced by layers 1, 2, and 3 of the architecture respectively. Magnitudes of blue and red lines are indicated by the left axis labels; magnitudes of orange and green lines are indicated by the right axis labels.

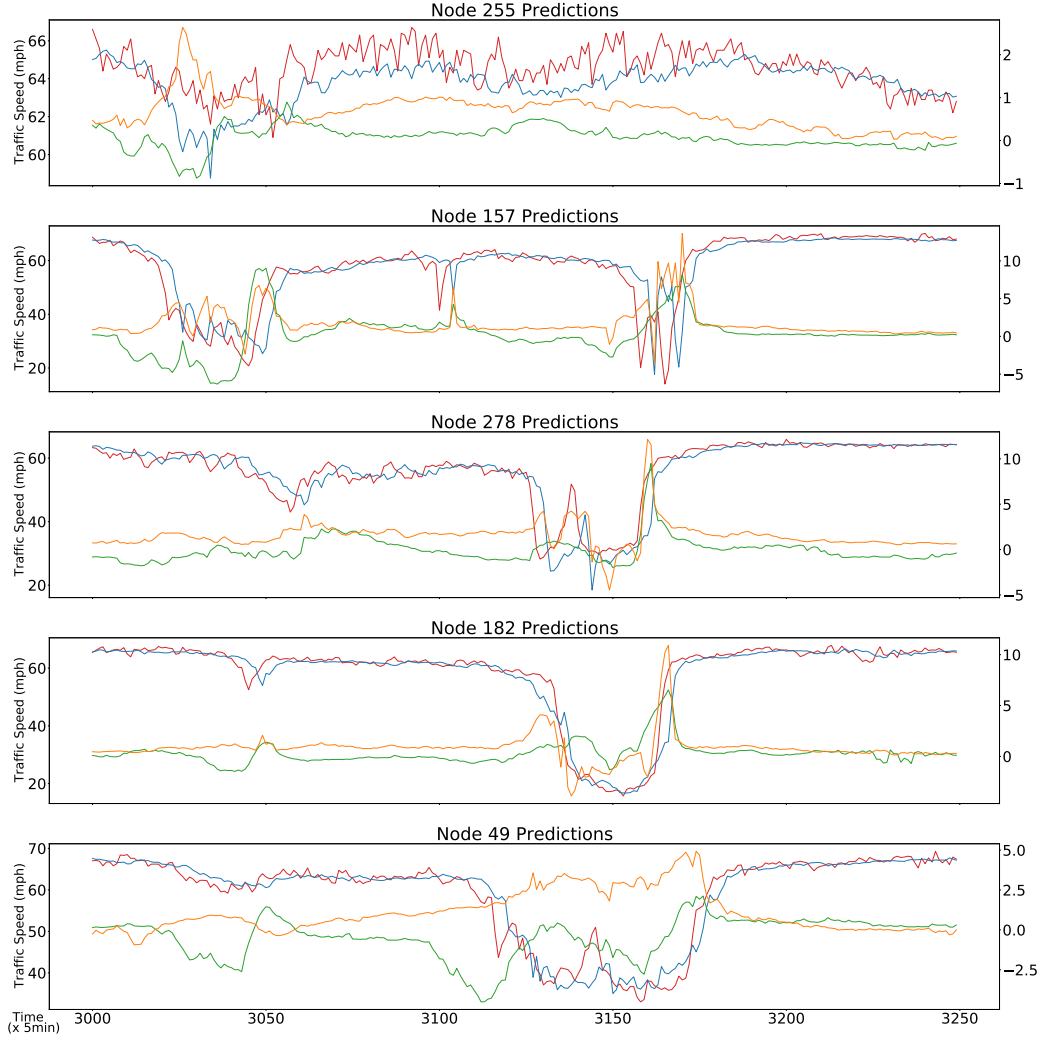


Figure 8: FC-GAGA 15 min ahead forecasts for different nodes in PEMS-BAY dataset from time 3000 to 3250. Blue, green and orange lines depict the partial forecasts produced by layers 1, 2, and 3 of the architecture respectively. Magnitudes of blue and red lines are indicated by the left axis labels; magnitudes of orange and green lines are indicated by the right axis labels.

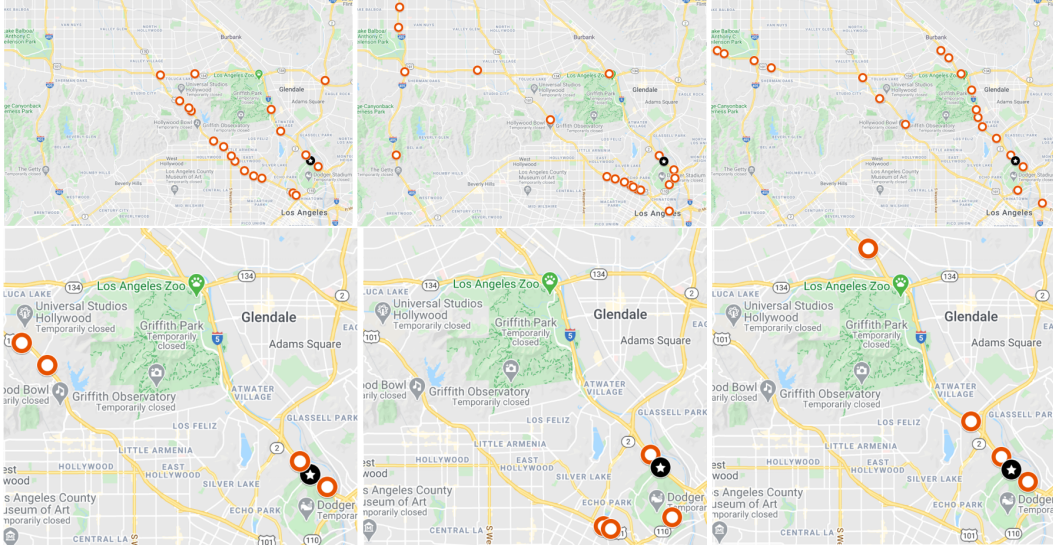


Figure 9: Maps of 20 and 4 highest weighted nodes for layers 1, 2, and 3 (left to right). The white star in the black circle is the forecasted node (node 101 in METR-LA).

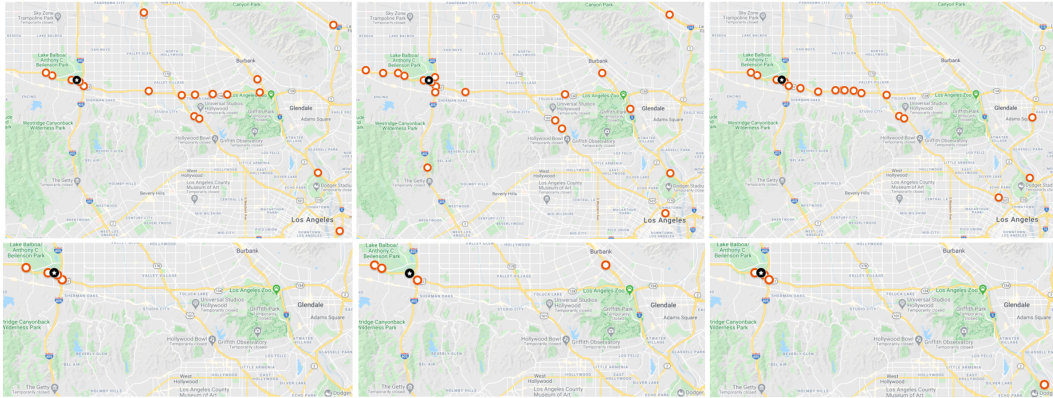


Figure 10: Maps of 20 and 4 highest weighted nodes for layers 1, 2, and 3 (left to right). The white star in the black circle is the forecasted node (node 146 in METR-LA).

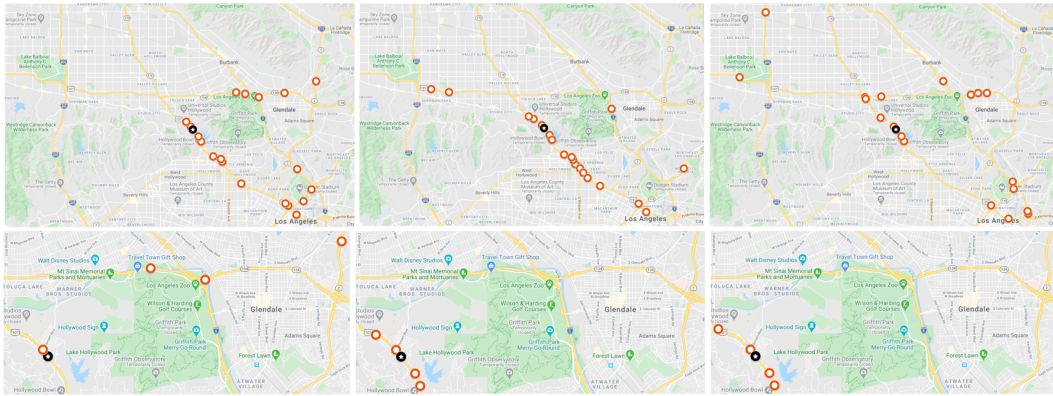


Figure 11: Maps of 20 and 4 highest weighted nodes for layers 1, 2, and 3 (left to right). The white star in the black circle is the forecasted node (node 39 in METR-LA).



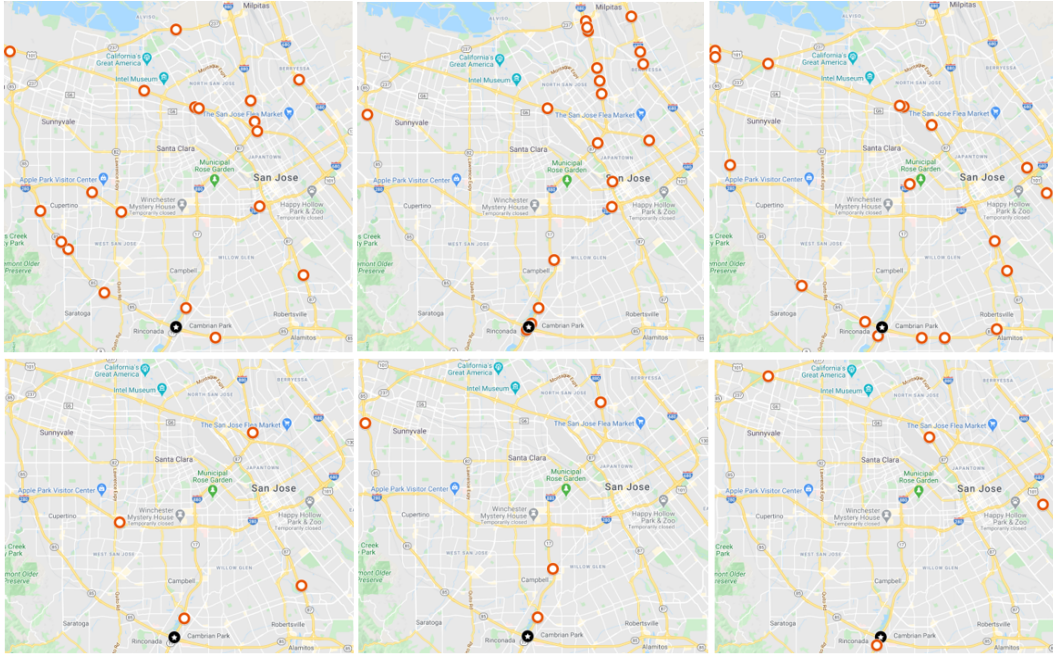


Figure 12: Maps of 20 and 4 highest weighted nodes for layers 1, 2, and 3 (left to right). The white star in the black circle is the forecasted node (node 10 in PEMS-BAY).

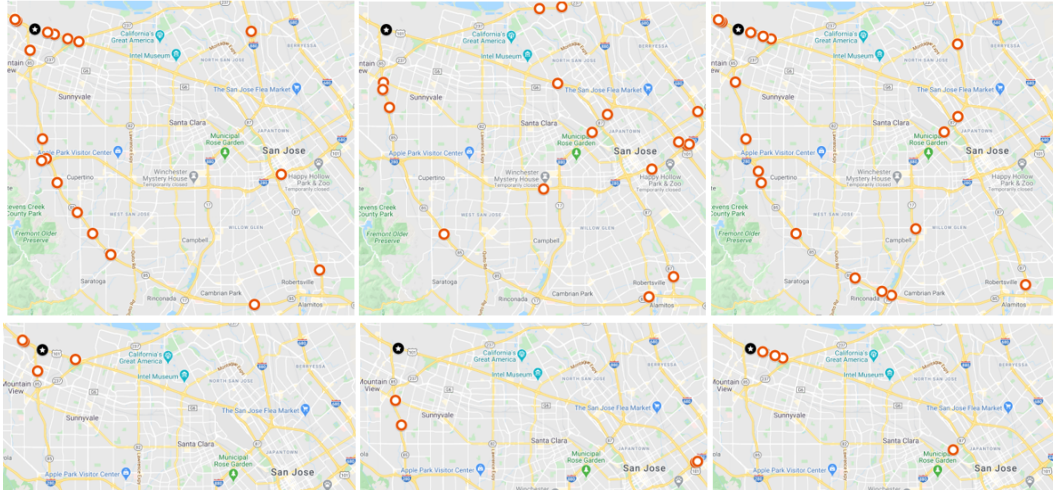


Figure 13: Maps of 20 and 4 highest weighted nodes for layers 1, 2, and 3 (left to right). The white star in the black circle is the forecasted node (node 179 in PEMS-BAY).



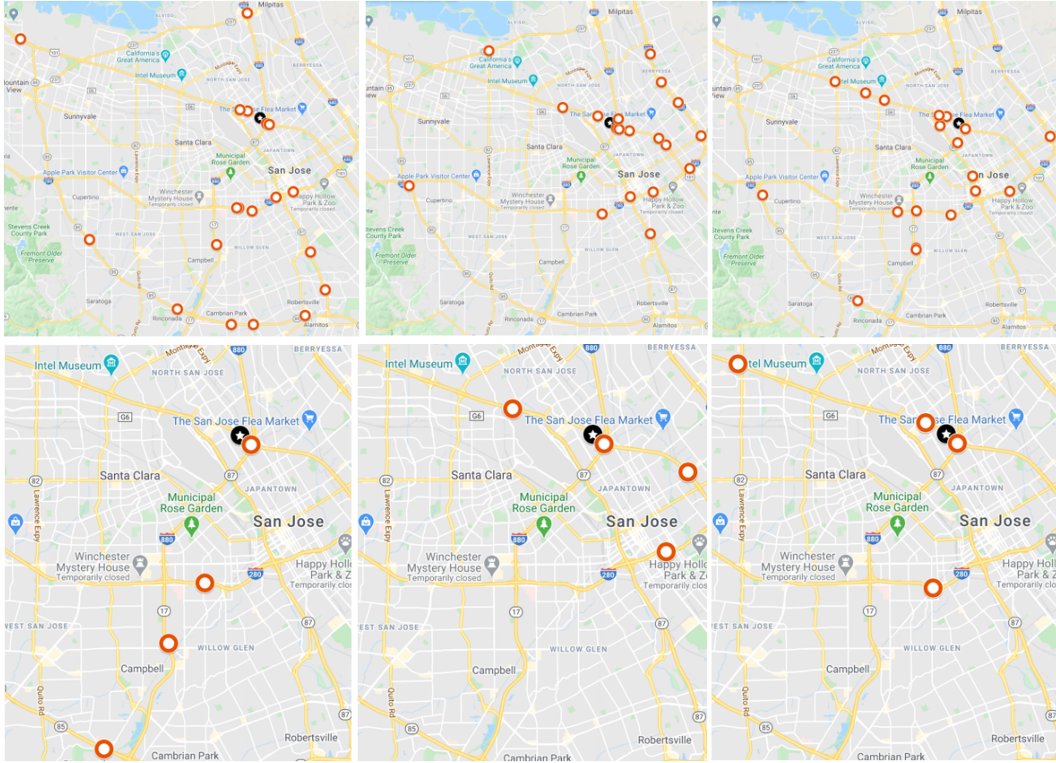


Figure 14: Maps of 20 and 4 highest weighted nodes for layers 1, 2, and 3 (left to right). The white star in the black circle is the forecasted node (node 216 in PEMS-BAY).

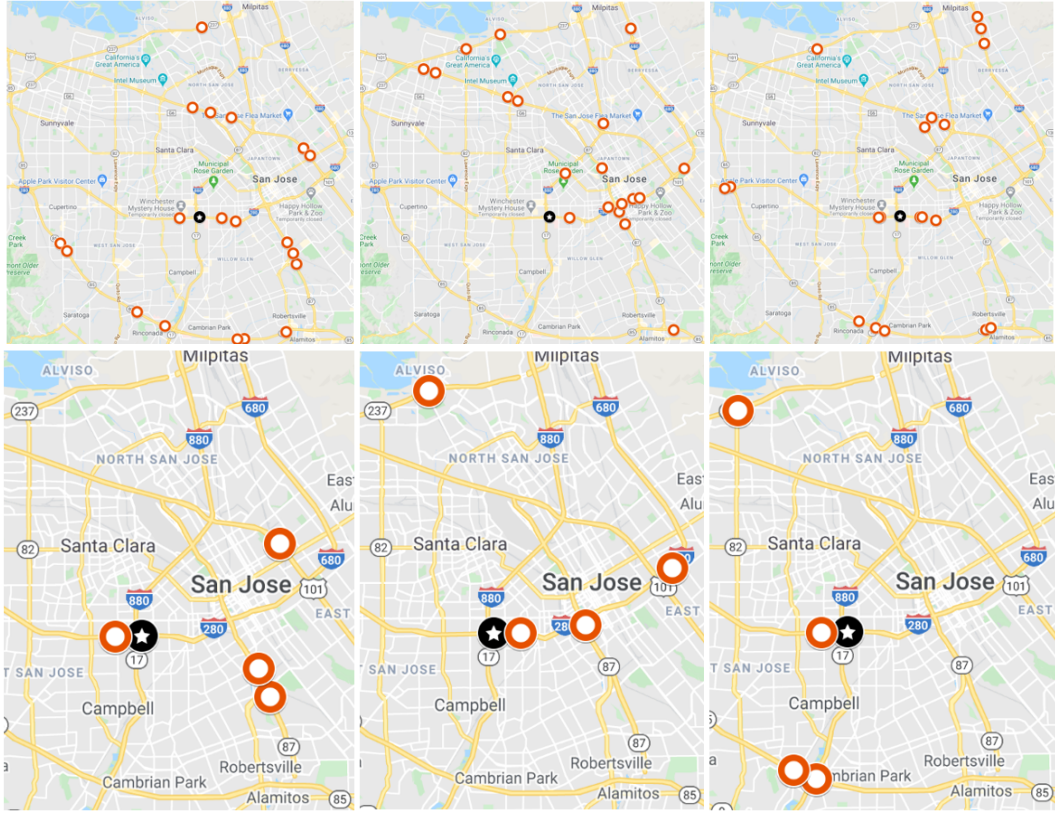


Figure 15: Maps of 20 and 4 highest weighted nodes for layers 1, 2, and 3 (left to right). The white star in the black circle is the forecasted node (node 310 in PEMS-BAY).

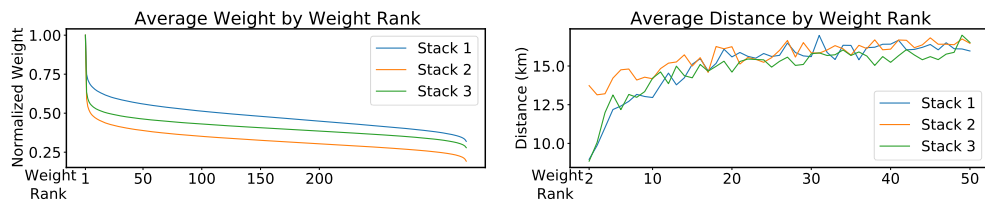


Figure 16: Average of graph gate weights  $\mathbf{W}_{i,j}$  normalized by the self-weight  $\mathbf{W}_{i,i}$  (left) and their average distances from the forecasted node (right) per FC-GAGA layer in PEMS-BAY dataset.